Plasma Impedance of Hall Effect Thrusters

IEPC-2025-675

Presented at the 39th International Electric Propulsion Conference
Imperial College London, London, UK
September 14-19, 2025

Kentaro Hara[1], Amy X. Zheng[2], Daniel E. Troyetsky[3],
Stanford University, Stanford, California 94305, USA

Janice D. Cabrera[4], Mitchell L. R. Walker[5],
Georgia Institute of Technology, Atlanta, GA, 30332, USA

Seth Thompson[6], John D. Williams[7],
Colorado State University, Fort Collins, CO 80523

The coupling between the power supply, circuit, and the plasma plays an important role in determining the dynamic behavior of electric propulsion (EP) systems. Typically, the discharge voltage and current are monitored in EP testing and operation. While the plasma dynamics is complex, the discharge voltage and current waveforms are affected by the plasma impedance, including resistive, capacitive, and inductive effects. We report how we can use experimental data to characterize the plasma impedance in EP systems.

I. Introduction

There is an increasing interest in understanding the facility effects of EP systems, as the technology matures and is deployed in actual missions in space. As shown in Fig. 1(a), in space, the thruster is not operated in a testing vessel, i.e., vacuum chamber, hence one of the most critical physical processes is how the ion beam is neutralized. Sufficient electron current needs to be provided such that the ion beam is neutralized and the satellite does not charge up. If the satellite is charged up, or if the ions return to the satellite, this means that net thrust is zero. Hence, beam neutralization is required for thrust generation.

The main three sources of facility effects that we we consider include (i) background pressure, (ii) electrical facility effects, and (iii) deposition of backsputtered materials from the vacuum chamber, as shown in Fig. 1(b). The key question is not whether facility effects exist; it is whether the facility effects influence the thruster operation. Even in the presence of the facility effects, if the discharge plasma, hollow cathode discharge and plume, and the thruster near-field plume are connected and are not affected by other factors, e.g., far-field plume, shorting, etc, then we can consider that the thruster will behave in space similar to ground tests.

What would be the perfect ground test that mimics a space-like condition? First, there is no ground in space. The reference electrical potential of interest is often considered to be the satellite common, because the main object of interest is the satellite itself. If the satellite common is at a lower voltage compared to the ambient plasma or plasma plume from the EP, this may indicate that some ions can be accelerated back to the satellite via a presheath and sheath. The floating condition, i.e., the EP system is floating with respect to the satellite common, can be established by having a large resistor between the cathode and satellite common (e.g., 100 MΩ). The large resistance will set up a voltage drop between the cathode and satellite common, which is supported by a negligibly small amount of current. For instance, if

[1]Assistant Professor, Aeronautics and Astronautics, kenhara@stanford.edu
[2]Undergraduate Student, Electrical Engineering, amyzheng@stanford.edu
[3]Ph.D. Candidate, Aeronautics and Astronautics, dtroyets@stanford.edu
[4]Ph.D. Candidate, School of Aerospace Engineering, Janice.d.cabrera@gatech.edu
[5]Professor, School of Aerospace Engineering, mitchell.walker@ae.gatech.edu
[6]Research Associate, Mechanical Engineering, Seth.Thompson@colostate.edu
[7]Professor, Mechanical Engineering, John.D.Williams@colostate.edu

the cathode-to-ground voltage is 20 V ann the resistance is 100 MΩ, the cathode-to-ground current is 0.2 μA, which is much smaller than the mean discharge current typically applied in EP systems (e.g., a few A). In fact, JAXA reported that their gridded ion engine faced a problem with the electrical effects since the loss of electrically conducting surfaces near that are connected to the satellite common resulted in a larger cathode voltage to maintain the designed current [1]. Second, the carbon materials are sputtered from beam dump in the vacuum chamber. These carbon particles can ballistically travel or can be electronically excited in the plume plasma, which may eventually lead to deposition inside the channel, on the pole piece, and thruster body. There are events where such deposited layers cause local shorting between electrical components that are designed not to be connected to the anode and cathode lines, which can change the thruster ignition and reliability. Third, the background neutrals that are reflected off of the chamber walls can come back to the thruster and elevate the neutral density and modify the neutral VDFs, particularly in the near-field plume region where neutrals from the anode are depleted due to the ionization in discharge channel. Experimental studies indicate that the neutral ingestion changes the cross-field electron mobility, leading to the shift of spatial locations of the ionization and acceleration region [2]. Depending on the ionization processes and the electrostatic potential profile, the thruster may experience a higher thruster efficiency with background pressure effects [3]. When designing the discharge voltage and current, this may necessitate decreasing or increasing the mass flow rate of neutral species. The community has generated recommended practices for facility testing [4]. It can also be considered that the background pressures may affect the electrical facility effects since the resistances between the cathode, thruster, and vacuum chamber can be affected the neutral gas residuals.

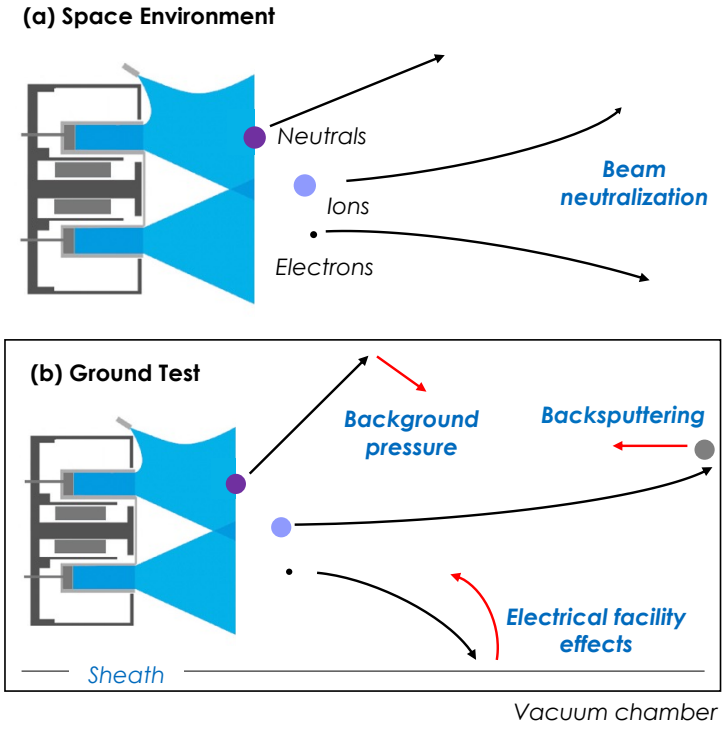

Fig. 1 Facility effects: in-space environment vs. vacuum chamber ground testing

In this paper, we are interested in analyzing the electrical responses of the plasma discharge. While high-fidelity physics-based models are necessary to advance our understanding of the plasma physics and chemistry [5], from a design and testing point of view, the voltage and current traces have the potential to provide us with information about the state, health, and life time of the thruster systems. In fact, one of the most easiest ways to detect something in the plasma discharge going wrong is through the voltage and current. For instance, if one sees a large voltage or current spike, one can speculate that arcing or an event that modified the electrical signals occurred.

Through this study, we reviewed several electrical engineering textbooks and papers [6] to figure out whether other communities proposed how to characterize complex electrical loads. While the impedance is typically evaluated as a complex number that describe the phase lag, almost all analyses assume that the capacitance, resistance, and

inductance of each circuit element remains constant in time. Using constant R, L, C, then impedance can be evaluated as a function of ω. This frequency is typically the frequency of the *excited* wave, either by applying a AC modulation at a given frequency or noise from various sources. We will report the circuit diagram, measurements, and the analysis of the effective resistance between anode and cathode. For instance, it is common to analyze the impedance of circuit components by applying an AC modulation in voltage or current to study its response. This technique is sometimes referred to as the RF I-V method in literature and has been used by David Jovel [7, 8]. In addition, harness impedance effects have been studied by Pinero [9] and Brieda [10]. In this paper, we discuss using the current and voltage waveforms to analyze the effective resistance, which we further analyze its amplitude and phase using Fourier transform.

II. Circuit

A. First-order band pass filter

The transfer function of an RC filter is known as

$$\frac{V_{out}(\omega)}{V_{in}(\omega)} = \frac{1}{1 + iRC\omega} = \frac{1 - iRC\omega}{\sqrt{1 + (RC\omega)^2}} \tag{1}$$

The cutoff frequency is known as $\omega = \omega_c = (RC)^{-1}$, where the amplitude drops off by $1/\sqrt{2} \sim 70$ %. This acts as a low-pass filter where the high-frequency signal at $\omega > \omega_c$ exponentially decays.

The transfer function of a LC filter can be derived as

$$\frac{V_{out}(\omega)}{V_{in}(\omega)} = \frac{1}{1 - (LC\omega)^2}. \tag{2}$$

Here, it can be seen that LC circuits produce the so-called resonant frequency: $\omega = (LC)^{-1/2}$. The output voltage would resonate and increase with respect to the input voltage without any resistance. In the presence of a resistance, the oscillations can be dampened.

B. Second-order band pass filter: RLC circuit

Figure 2 shows a typical RLC circuit. When all circuit components are invariant in time, one can write the following equations:

$$I_{out} = I - C\frac{dV_{out}}{dt} \tag{3}$$

$$V_{out} = V_{in} - IR - L\frac{dI}{dt} \tag{4}$$

Hence,

$$V_{in} = V_{out} + \left(I_{out} + C\frac{dV_{out}}{dt}\right)R + L\frac{d}{dt}\left(I_{out} + C\frac{dV_{out}}{dt}\right) = I_{out}R + L\frac{dI_{out}}{dt} + V_{out} + RC\frac{dV_{out}}{dt} + LC\frac{d^2V_{out}}{dt^2}, \tag{5}$$

which is a second-order differential equation. It can be seen that the transfer function of a LC filter can be obtained only when $L = 0$ and $I_{out} = 0$ and the transfer function of a LC filter can be obtained only when $R = 0$ and $I_{out} = 0$. If there is a plasma load for the output end, one can consider a plasma load:

$$R_{\text{eff}}(t) = \frac{V_{out}(t)}{I_{out}(t)}. \tag{6}$$

Thus, $I_{out} = 0$ can only be achieved then $R_{\text{eff}} \to \infty$.

This example of a RLC circuit exhibits that the governing equation of the entire circuit system must be constructed to understand the impact of each electric circuit components. In the presence of a plasma load, the voltage relation can be written as

$$V_{in} = \frac{V_{out}}{R_{\text{eff}}}R + L\frac{d}{dt}\left(\frac{V_{out}}{R_{\text{eff}}}\right) + V_{out} + RC\frac{dV_{out}}{dt} + LC\frac{d^2V_{out}}{dt^2}. \tag{7}$$

It is evident that only in a linear system with time-invariant circuit elements including constant R_{eff}, one can take a Fourier / Laplace transform and evaluate the transfer function as a function of a frequency. For instance, $V_{in}(\omega) = \text{FFT}[V_{in}(t)]$ and $V_{out}(\omega) = \text{FFT}[V_{out}(t)]$. If R, L, C, R_{eff} are all constant (i.e., time-invariant), then it can be seen that $V_{in}(\omega)$ is linearly dependent on $V_{out}(\omega)$. Thus, the transfer function is uniquely defined for a given frequency ω.

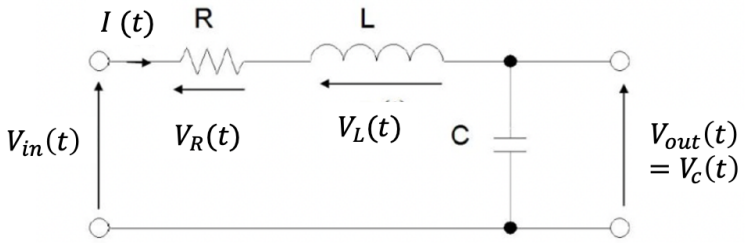

Fig. 2 RLC circuit. The input current and voltage are $I(t)$ and $V_{in}(t)$. The output current and voltage are $I_{out}(t)$ and $V_{out}(t)$.

C. H9 testing in Georgia Tech vacuum chamber

Figure 3 shows the electric circuit elements from the power supply (ps) to the Hall effect thruster (HET) plasma, cathode plasma, plume plasma, and ground (i.e., chamber wall). The circuit values are obtained by D. Jovel during his thesis study [8] using an external voltage perturbation with a given frequency. This technique is also known as the RF I-V method. Further, J. Cabrera analyzed that the output current due to the perturbed voltage is observed at the same frequency as the excitation.

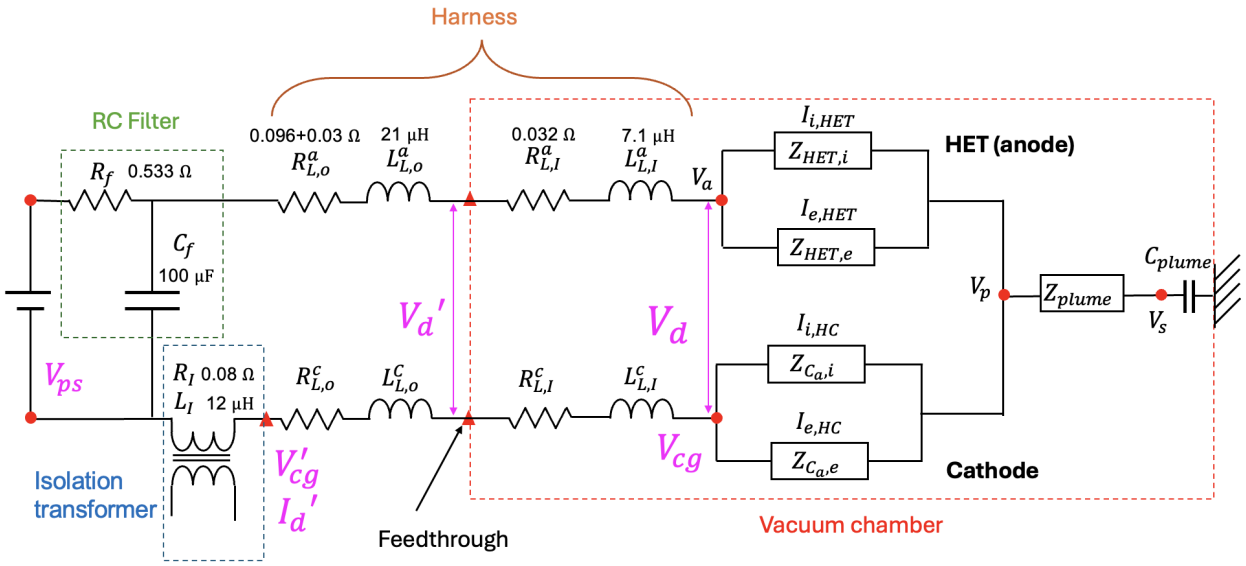

Fig. 3 Circuit diagram of the H9 testing at Georgia Tech. The prime quantities denote where the measurements are taken.

III. Impedance characterization

The data of a H9 thruster were collected by J. Cabrera in March and April 2024, operated in Georgia Institute of Technology. The measurements included discharge voltage (V_d'), discharge current (I_d'), and cathode-to-ground voltage (V_{cg}') for this testing campaign. We are interested in using the telemetry data to characterize the thruster performance.

A. Experimental data: V_d and I_d

Figure 4 shows the experimental data of the discharge voltage and discharge current. The actual data set collected include 100 ms worth of data. In Figs. 4(a,b), we select a 2 ms window to show the discharge voltage and current

oscillations more clearly. The mean values are 300 V and 20 A. The oscillation amplitude is approximately 30-40 V and 6-7 A. The discharge current and voltage data acquisition is performed synchronously. Now, we can take a fast

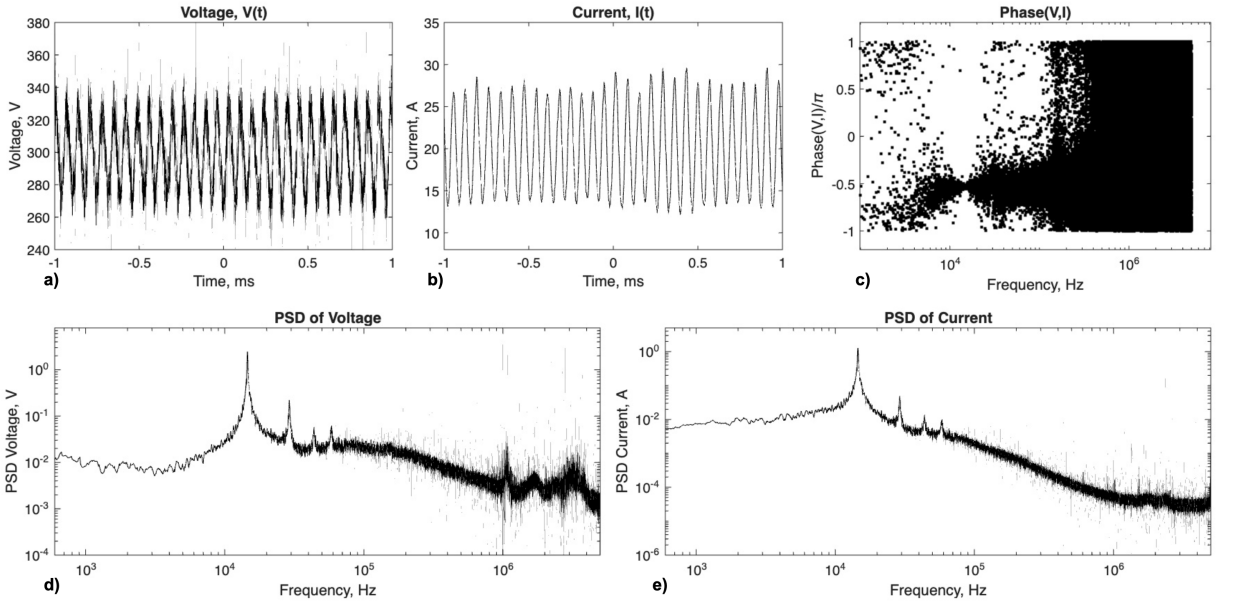

Fig. 4 Thruster data for the 300 V 20 A operation with ground thruster body: (a) Discharge voltage time series $V_d(t)$, (b) Discharge current time series $I_d(t)$, (c) Phase between V_d and I_d, (d) power spectral density (PSD) of discharge voltage, $|V_d(\omega)|$, and (e) PSD of discharge current, $|I_d(\omega)|$.

Fourier transfer (FFT) of the time series, which yield complex numbers for the frequency series. A time series data, e.g., $F(t)$, translates to FFT$[F(t)] = F_R(\omega) + iF_I(\omega) \equiv \tilde{F}(\omega)$, where tilde indicates that $\tilde{F} \in \mathbb{C}$, $F_R \in \mathbb{R}$, $F_I \in \mathbb{R}$, and i is the imaginary number. The amplitude of the FFT data can be calculated as $|\tilde{F}| = \sqrt{F_R^2 + F_I^2}$. The phase can be calculated as $\theta = \tan^{-1}(F_I/F_R)$. Figure 4(c) is the phase between V_d and I_d. It is interesting that there is a -90° phase shift between V_d and I_d around the strongest oscillation mode at 15 kHz, cf. breathing mode. The phase starts to broaden at higher frequency. The phase seems a bit more chaotic (i.e., can see signature at all phases) around 150 kHz. The oscillation amplitudes of V_d and I_d are shown in Figs. 4(d,e). Since the voltage and current oscillation is no longer a small-amplitude signal, the PSDs show that the higher harmonic oscillation modes are present (cf. nonlinear oscillation). At lower power, e.g., 300 V and 15 A, the oscillations were found to be smaller in amplitude, in which case the PSDs do not show the higher harmonic modes.

B. Effective Resistance: $R_{\text{eff}} = V_d/I_d$

As shown in Fig. 1, the discharge current and voltage between the anode and cathode contains several plasmas, including Hall effect thruster (HET) discharge plasma, near-field plume where the HET and hollow cathode plasmas are connected, and hollow cathode plasma. Each plasma can potentially possess resistive, capacitive, and inductive components. However, it is important to note that the discharge voltage and current are *real* numbers as a function of time. In addition, discharge current is technically defined at the anode and cathode surface since it is the number of *charges* (both ions and electrons) per second that are absorbed at the electrode. Typically, if one runs a numerical simulation of a HET discharge plasma, the net current is typically constant in the domain since the electrons can immediately adjusts there movement via the electric field. Assuming that the current is uniformly passing through the HET, plume, and hollow cathode plasmas, then we can consider the effective resistance between the anode and cathode as, $R_{\text{eff}}(t) = V_d(t)/I_d(t)$.

Figure 5(a) shows the effective resistance as a function of time. The mean value is at 15 Ω, but the profile seems asymmetric around the mean value, i.e., the minimum and maximum values are approximately 10 Ω and 25 Ω, respectively. This is because the waveform of R_{eff} is not sinusoidal. In fact, the PSD of R_{eff} is shown in Fig. 5(b), where the 2nd and 3rd harmonic modes are visible. There are also features around 1 MHz, which is visible in the discharge

voltage PSD in Fig. 4(d) but not in the discharge current in Fig. 4(e). To be complete, we also show the phases of the effective resistance with respect to the discharge current and voltage in Figs. 5(c,d), respectively. It can be seen that there is an approximately -160° phase between R_{eff} and I_d, which is close to ±180°. The phase between R_{eff} and V_d is approximately −70°. In both Figs. 5(c,d), between the dominant and 2nd harmonic modes, the phase seems to primarily shift upwards, while a small signal goes the opposite direction. While the phases may contain some useful plasma information, we reserve such analyses for future investigations.

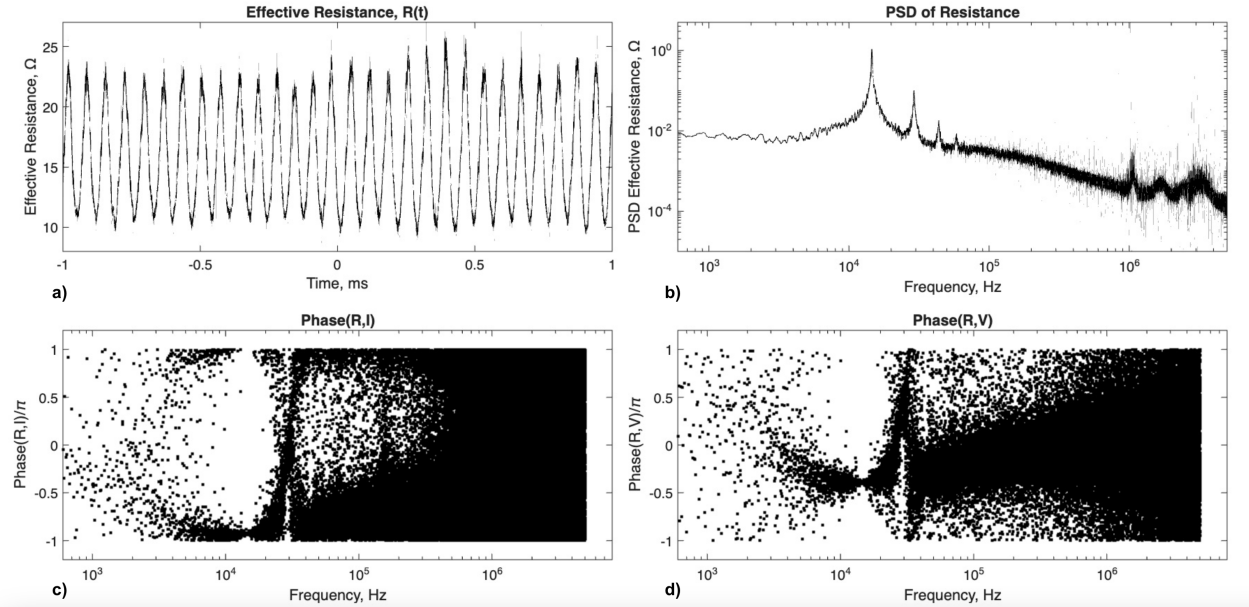

Fig. 5 Analysis using the 300 V 20 A dataset with ground thruster body: (a) effective resistance time series, $R_{\text{eff}}(t)$, (b) PSD of effective resistance, $|\tilde{R}_{\text{eff}}(\omega)|$, (c) phase between R_{eff} and I_d, and (d) phase between R_{eff} and V_d.

C. Different operating conditions

Figure 6 shows the analysis of the effective resistance between the anode and cathode for different operating conditions with cathode-tied thruster body.

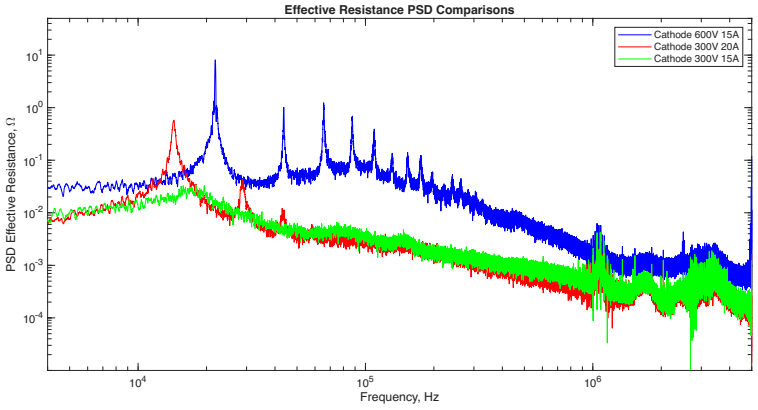

Fig. 6 Effective resistance comparisons for different voltage and current ratings in the cathode configuration. Cathode tied configuration.

The 4.5 kW (300 V 15 A) case shows the smallest oscillation and no harmonics. The 6 kW (300 V 20 A) case shows similar PSD compared to the 4.5 kW case, but the peak is slightly larger and some harmonic modes are excited. Even the high-frequency MHz oscillations show agreement between the 4.5 kW and 6 kW cases. On the other hand, the 9 kW

condition (600 V and 15 A) is quite different from the 300 V discharge. There are many more harmonic oscillations (up to 9th). The excitation of such higher-order harmonic oscillations is likely responsible for the spectra in 100 kHz to 1 MHz to be elevated compared to the 4.5 kW and 6 kW cases. Higher discharge voltage would imply that the discharge current oscillation is highly nonlinear to a point where the discharge can be considered unstable [11]. This occurs since the ionization rate is the source term for the ions and the advection is the sink term for the ions. The 0D globally averaged ion continuity equation can be written as

$$\frac{\partial N_i}{\partial t} + \frac{U_i}{L} = N_n k_{ion}(T_e), \tag{8}$$

where N_i is the ion density, U_i is the ion bulk velocity at the exit, L is the ionization length, N_n is the neutral atom density, k_{ion} is the ionization rate coefficient which is a function of the electron temperature, T_e. For krypton with 600 V, the characteristic ion bulk velocity is $U_i = 38$ km/s. If assuming $L = 0.01$ m, then the loss frequency is 3.8 MHz. If $N_n \sim 10^{19}$ m^{-3} and $k_{ion} \approx 10^{-14}$ m^3/s, then ionization frequency is 0.1 MHz, which means that there is no *steady-state* ion discharge. In such a condition, the discharge is forced to experience a large-amplitude discharge oscillation.

IV. Background pressure study

With the same thruster in the same vacuum chamber, the H9 was operated. We compare the March and April data sets.

A. March dataset

Figure 7 shows (a) the effective resistance in time, (b) the PSD of effective resistance, (c) PSD of discharge voltage, and (d) PSD of discharge current. From all the results it can be seen that the peak is weakened with larger pressure. In addition, the frequency is slightly shifted to a smaller number. Based on the 0D analysis [11], the breathing mode frequency can be written as $\omega_0 = \sqrt{U_i U_n}/L$ or $\omega_0 = \sqrt{N_i N_n k_{ion}^2}$. One explanation of the change in the breathing mode frequency is decrease in U_i or increase in L. The other explanation is T_e decreases with higher background pressure.

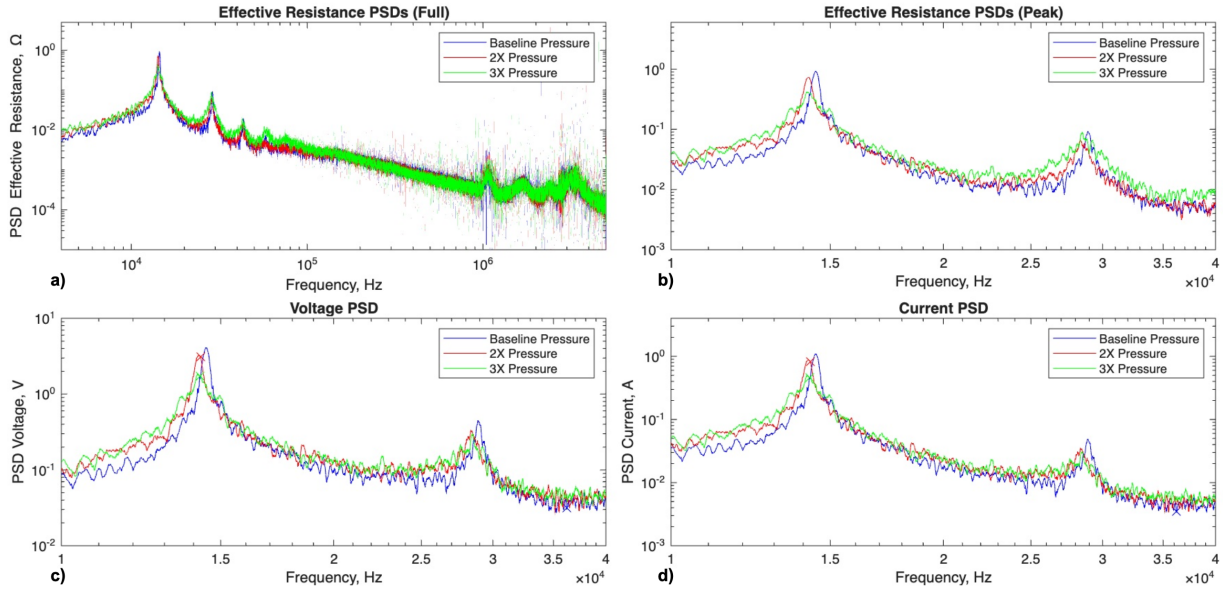

Fig. 7 March dataset with ground thruster body: (a) effective resistance PSDs in full range, b) zoomed-in effective resistance PSDs, c) zoomed-in voltage PSDs , and d) zoomed-in current PSDs.

Figure 8 shows the phase between V_d and I_d as well as the phase between R_{eff} and I_d. The $V_d - I_d$ phase can be compared to the March data in Fig. 4(c), showing similar results. The $R_{\text{eff}} - I_d$ phase is also comparable to Fig. 5(c).

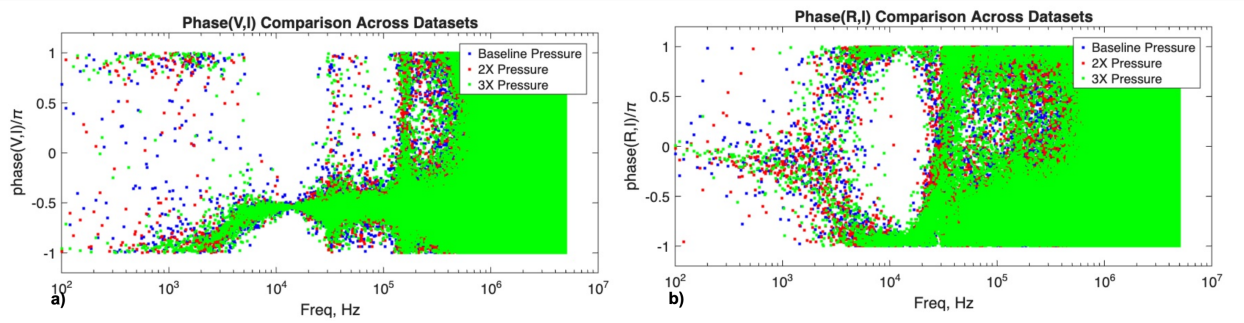

Fig. 8 March dataset with ground thruster body: (a) $V_d - I_d$ phase and (b) $R_{\text{eff}} - I_d$ phase.

B. April dataset

Figure 9 shows the background pressure study for the April dataset with floating thruster body. It was observed that the discharge voltage oscillation peaks around 15 kHz but the discharge current oscillation peaks around 55 kHz for most of the data in the April test, which is starkly different from the March data set where the voltage and current oscillations were more aligned. Not only the dominant frequency is shifted but also the discharge current oscillation amplitude is much smaller in the April test. The 50-60 kHz, small-amplitude discharge current oscillation is actually consistent with other SPT and PPPS series observations. For instance, Gascon showed that at nominal 300 V condition, the breathing mode oscillation jumps to 50 kHz and the dominant frequency is approximately 20 kHz below and above 300 V. The same trend was also reported by Tsikata with the PPPS-1350 data taken in CNRS [12].

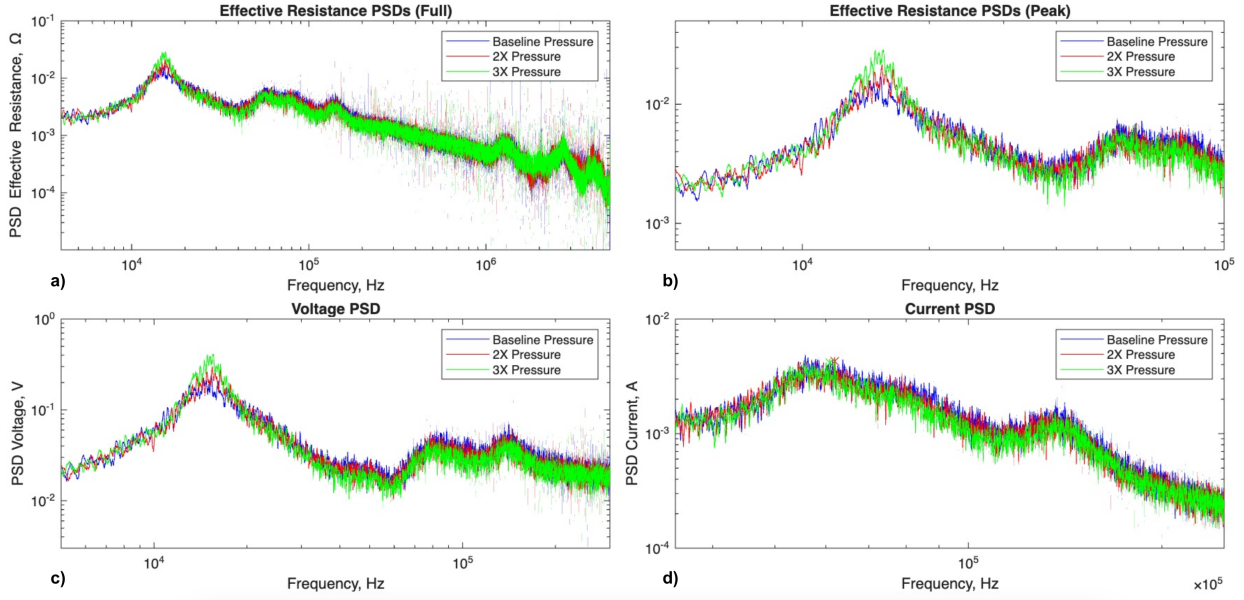

Fig. 9 April dataset with floating thruster body: (a) effective resistance PSDs in full range, b) zoomed-in effective resistance PSDs, c) zoomed-in voltage PSDs, and d) zoomed-in current PSDs.

The March test, as shown in Fig. 7(a), shows the oscillation amplitude of plasma resistance reaches 1 Ω. However, the April test shown in Fig. 9(a), the peak is smaller. For the floating condition during the April test, it is observed that the breathing mode frequency actually increases as the background pressure increases. This is an opposite trend compared to the March test. More investigation is required.

Figure 10 shows (a) the phase between V_d and I_d and the phase between R_{eff} and I_d. The phase profiles are very different from the March tests. The phase before 15 kHz and the phase between 15 kHz and 55 kHz seem different. For instance, below 15 kHz spectra show a -90° degree shift between V_d and I_d, which is similar to the March tests.

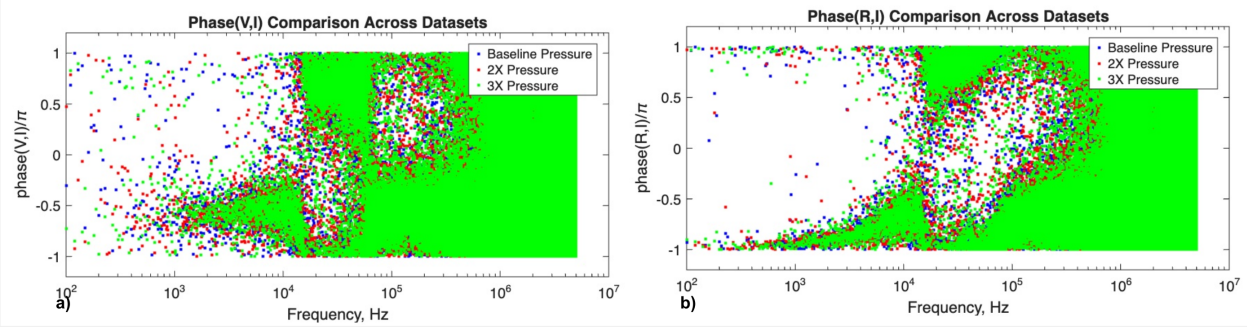

Fig. 10 April dataset with floating thruster body: (a) $V_d - I_d$ phase and (b) $R_{\text{eff}} - I_d$ phase.

However, the spectrum between 15 kHz and 55 kHz shows a phase around +90°. The phase above 55 kHz seems consistent with the other test results. One speculation is that there is a difference in the anode current and cathode current. Since the data taken were on the cathode line, the cathode current could consist of the electrons that move toward the HET as well as the electrons that close another circuit toward the chamber wall. We are investigating the causality of such changes.

V. Conclusion

In this paper, we are proposing that the plasma impedance (or strictly speaking, the effective resistance) contains useful information about the current paths, which may lead to gaining better understanding of electrical facility effects. The plasma effective resistance as a function of time is calculated based on the discharge current and voltage obtained from the measurement. Then, the time-series resistance is analyzed using the fast Fourier transform. The phase and the amplitude of the complex signal are analyzed for different thruster operating conditions and thrust body configurations.

Acknowledgments

This work was supported by NASA through the Joint Advanced Propulsion Institute. The first author thanks the discussions with David Jovel, Ajay Krishnan, Yusuke Yamashita, Maryam Saeedifard, John Yim, Mark Cappelli, and Juan Rivas. The first and second authors appreciate the support from the Research Experience for Undergraduate (REU) program in the Department of Aeronautics and Astronautics at Stanford University.

References

[1] Nono, A., Morishita, T., Hosoda, S., Tsukizaki, R., and Nishiyama, K., "Effect of spacecraft surface conductivity on voltage of microwave neutralizer in gridded ion thrusters," *Acta Astronautica*, Vol. 212, 2023, pp. 130–138.

[2] Huang, W., and Kamhawi, H., "Facility Effects on the Ion Characteristics of a 12.5-Kilowatt Hall Thruster," *Journal of Propulsion and Power*, Vol. 39, No. 5, 2023, pp. 665–674.

[3] Diamant, K. D., Liang, R., and Corey, R. L., "The effect of background pressure on SPT-100 Hall thruster performance," *50th AIAA/ASME/SAE/ASEE Joint Propulsion Conference*, 2014, p. 3710.

[4] Dankanich, J. W., Walker, M., Swiatek, M. W., and Yim, J. T., "Recommended practice for pressure measurement and calculation of effective pumping speed in electric propulsion testing," *Journal of Propulsion and Power*, Vol. 33, No. 3, 2017, pp. 668–680.

[5] Hara, K., "An overview of discharge plasma modeling for Hall effect thrusters," *Plasma Sources Science and Technology*, Vol. 28, No. 4, 2019, p. 044001.

[6] Barsoukov, E., and Macdonald, J., *Impedance Spectroscopy: Theory, Experiment, and Applications*, Wiley, 2018. URL `https://books.google.com/books?id=7udRDwAAQBAJ`.

[7] Jovel, D. R., Cabrera, J. D., and Walker, M. L., "Current pathways model for hall thruster plumes in ground-based vacuum test facilities: measurements and observations," *Journal of Electric Propulsion*, Vol. 3, No. 1, 2024, p. 35.

[8] Jovel, D. R., Cabrera, J. D., and Walker, M. L., "Hall effect thruster impedance characterization in ground-based vacuum test facilities," *Journal of Electric Propulsion*, Vol. 3, No. 1, 2024, pp. 1–26.

[9] Piñero, L. R., "The impact of harness impedance on Hall thruster discharge oscillations," *International Electric Propulsion Conference*, 2017.

[10] Brieda, L., Koo, J., and Scharfe, M., "Influence of a power supply model on simulated Hall thruster discharge voltage oscillations," *AIP Advances*, Vol. 9, No. 2, 2019, p. 025320. https://doi.org/10.1063/1.5063440.

[11] Hara, K., Sekerak, M., Boyd, I., and Gallimore, A., "Perturbation analysis of ionization oscillations in Hall effect thrusters," *Phys. Plasmas*, Vol. 21, 2014, p. 122103. https://doi.org/10.1063/1.4903843.

[12] Troyetsky, D., Greve, C., Tsikata, S., and Hara, K., "State estimation of the dynamic behavior of plasma properties in a Hall effect thruster discharge," *Journal of Physics D: Applied Physics*, Vol. 56, No. 44, 2023, p. 444001.